Giant dipole resonance decay from fusion-fission and quasifission of hot thorium nuclei

I. Diószegi,* D. J. Hofman, C. P. Montoya, S. Schadmand, and P. Paul
Department of Physics, State University of New York at Stony Brook, Stony Brook, New York 11794
(Received 23 March 1992)

Giant dipole resonance (GDR) γ rays were measured in kinematic coincidence with fission fragments in the reactions $^{16}O+^{208}Pb$ at 140 MeV, and $^{32}S+^{nat}W$ at 185, 215, and 230 MeV bombarding energy, leading to $^{\sim 216,224}Th$ at a temperature of $T \approx 1.8$ to 2.1 MeV. The experiment determined the γ-ray spectrum and the γ-ray-fission fragment angular correlation as a function of fragment mass, kinetic energy, and total kinetic energy release. The coincidence γ-ray spectra are fitted successfully and consistently in terms of the statistical decay of the hot compound system and of the fission fragments, when a large nuclear dissipation ($\gamma = 10$) and, for the $^{32}S+^{nat}W$ reaction, the GDR γ emission during the quasifission process is included. The γ-ray-fission fragment angular correlation indicates a deformed compound system in ^{224}Th of either strongly prolate ($\beta = 0.3$) or noncollective oblate ($\beta = -0.1$) shape. This is consistent with, but does not prove, a transition to a liquid drop shape having occurred at $T \approx 1.8$ MeV. The quasifission process is successfully included using regular extra-push and extra-extra-push energies and a quasifission lifetime $\tau_{QF} = (20-40) \times 10^{-21}$ sec. This is about ten times shorter than the compound nucleus fission lifetime in ^{224}Th at this temperature.

PACS number(s): 25.70.Jj, 25.70.Gh, 24.30.Cz

I. INTRODUCTION

In a series of previous papers [1,2] the γ decay from the giant dipole resonance (GDR) in hot thorium nuclei has been used to investigate the time scale of the compound nucleus (CN) fission process. In a hot nucleus GDR γ rays are emitted in the early steps of the CN decay with a total strength given by one classical dipole sum rule. In heavy systems, where the residue cross section is small compared to the fission cross section, the measured γ-ray spectrum contains not only the prefission γ rays from the CN GDR but also postfission statistical and GDR γ rays from the deexciting fission fragments. Thus one can deduce the fission time by extracting the amount of prefission GDR γ rays relative to post-fission γ rays through fits to the measured total γ-ray energy spectrum. Using this method [2] with the 140 MeV $^{16}O+^{208}Pb$ reaction (which forms ^{224}Th) enabled the extraction of a total fission time scale $\tau_{fiss} \sim 2.9 \times 10^{-19}$ s at an initial nuclear temperature of ~ 1.8 MeV. However, when the thorium system is formed in the more symmetric reaction $^{32}S+^{nat}W$, the quasifission process becomes comparable in strength to CN fission [3], leading to a more complicated situation.

Previously [2] the reaction $^{32}S+^{nat}W$ (which forms $^{214,216,218}Th$) was studied at 185 MeV, to explore whether GDR γ decay could be used to learn about the time scale of the quasifission process or about the deformation of the quasifissioning system (the mononucleus). Indeed, it was found that inclusion of the quasifission process, in addition to CN fission, helped to describe the measured γ-ray energy spectra and γ-ray-fission angular correlation. The observation of an anisotropy in the GDR γ emission with respect to the spin axis of the intermediate $^{\sim 216}Th$ system indicated that the system lives long enough to emit GDR γ rays prior to scission, and this fact was then used to extract an approximate quasifission lifetime, $\tau_{QF} = (2-9) \times 10^{-20}$ s. To fit the γ spectrum, however, an arbitrary reduction of the fission fragment excitation energy was necessary.

The present measurements are intended to look for quasifission effects in more detail, i.e., as a function of excitation energy, and also to investigate the nuclear viscosity as a function of the nuclear temperature. To this end the experimental setup was upgraded with multiwire avalanche counters which allow detection of the fission fragments in kinematic coincidence and to determine their masses and energies through a time-of-flight measurement, in coincidence with high-energy γ rays. In addition to new measurements of the $^{32}S+^{nat}W$ reaction, the $^{16}O+^{208}Pb$ reaction was revisited in order to take advantage of the improvements in the experimental setup which are intended to make a better background discrimination and thus yield a cleaner γ-ray energy spectrum.

II. EXPERIMENTAL PROCEDURE

The production of high-energy γ rays in the $^{16}O+^{208}Pb$ and $^{32}S+^{nat}W$ reactions was studied using pulsed ^{16}O and ^{32}S beams from the Stony Brook LINAC. The most important properties of the systems investigated in the present series of experiments are listed in Table I. The beam repetition time was 106 ns with an average pulse width of ~ 800 ps. The $^{16}O+^{208}Pb$ reaction was performed with a ~ 5 particles nA (p nA) 140 MeV ^{16}O beam incident on a self-supporting ^{208}Pb target of thickness 800 $\mu g/cm^2$. The $^{32}S+^{nat}W$ reaction was studied at

*On leave from Institute of Isotopes of the Hungarian Academy of Sciences, H-1525 Budapest, P.O. Box 77, Hungary.

TABLE I. Summary of the investigated compound systems. The columns list the reaction, compound nucleus (CN), beam energy E_{lab} (MeV), excitation energy E^*_{CN} (MeV) of the CN, initial nuclear temperature T (MeV) of the CN, average energy E^+ (MeV) at the scission point, total fusion cross section σ_{tot} (mb) and the corresponding maximum angular momentum l_{max} ($\hbar$).

Reaction	CN	E_{lab}	E^*_{CN}	T	E^+	σ_{tot}	l_{max}
$^{16}O+^{208}Pb$	^{224}Th	140	82	1.8	85	1500[a]	65
$^{32}S+^{nat}W$	$^{214,216,218}Th$	185	72	1.7	73	449[b]	53
		215	97	2.0	98	725[b]	73
		230	110	2.1	111	1004[b]	89

[a]Cross-section data extrapolated from results of [23].
[b]Cross-section data of [3].

three ^{32}S beam energies of 185, 215, and 230 MeV, at currents of ~ 3 p nA. The same self-supporting ^{nat}W target of thickness 675 $\mu g/cm^2$ was used for these three experiments. In all cases the target was placed at 45° to the beam axis and tilted 45° from the vertical position.

γ rays in coincidence with both fission fragments were detected using a shielded 25.4 cm×38.1 cm cylindrical NaI(Tl) detector [4] and four 19.8 cm×4.9 cm position sensitive parallel plate avalanche counters (PPAC's) [5] mounted in a lamp shade geometry around the target (see Fig. 1). As in prior measurements, the NaI detector was placed 90° to the beam direction, with its front face at 60 cm from the target for good time-of-flight (TOF) separation between γ rays and neutrons. The energy calibration of the NaI detector was obtained from the $^{11}B(p,\gamma)$ reaction at $E_p = 7.00$ MeV [4].

The four position sensitive PPAC's were positioned such that one pair defined a mid-plane perpendicular to the NaI detector axis, and the other a collinear one. This permitted the measurement of kinematically coincident fission fragments, in coincidence with γ rays emitted either parallel (0°) or perpendicular (90°) to the spin axis of the intermediate system [7]. With a closest distance from the target of 16.0 cm, each fission detector covered laboratory polar angles of $30° < \theta < 95°$ relative to the beam axis and azimuthal angles of $-7.5° < \phi < +7.5°$.

The PPAC's consisted of two separate set of cathode-wire grid pairs, which determined the impact points of the fission fragments and elastically scattered particles on the detector surface [5]. The position information was obtained from the wire grids by the charge division method, with a resolution of ~ 2.5 mm as determined with a ^{252}Cf source. The signal from the first cathode provided the timing trigger. Figure 2 shows a time-of-flight spectrum for one of the detectors, displaying the elastically scattered ^{32}S beam, fission fragments and W recoils. A time resolution of 1.1 ns was determined from the TOF spectrum of the elastically scattered ^{32}S ions.

All analog and timing signals were integrated and digitized using FERA CAMAC modules and written event by event on magnetic tapes. Pileup events were filtered out from the γ-ray energy data as described earlier [4,6].

The position and time information for the fission fragments were translated into fragment masses and velocity vectors off line by use of a kinematic coincidence method developed by Casini *et al.* [8]. In this method, the primary fragment masses and original velocity vectors are extracted using the fact that there is an overdetermina-

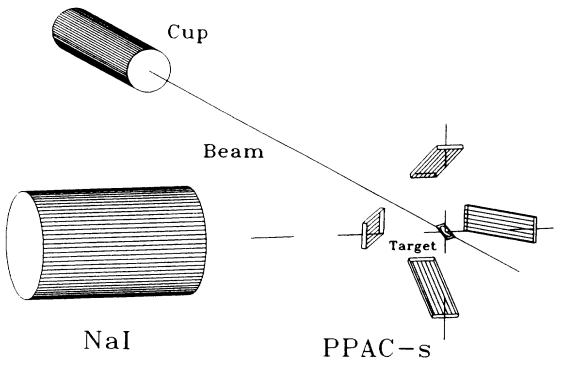

FIG. 1. The experimental setup showing the shielded NaI detector and the four position sensitive PPAC detectors.

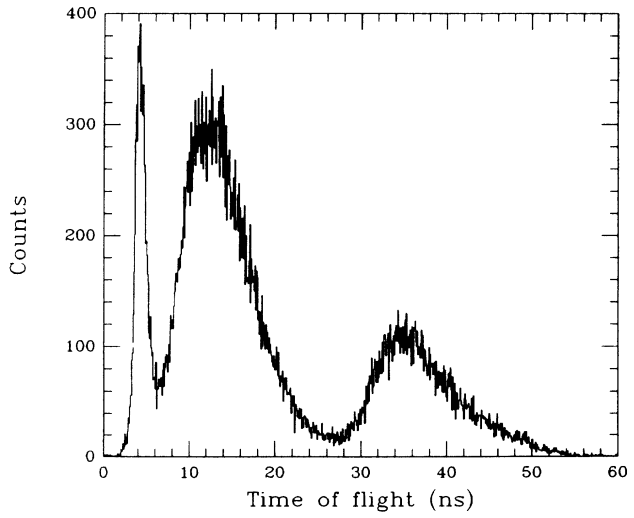

FIG. 2. Time-of-flight spectrum, measured by the top PPAC detector. The spectrum contains events from a 1 cm×1 cm area of the PPAC. The three peaks correspond to elastically scattered ^{32}S and ^{181}W (left and right peaks), and fission fragments (wide peak in the middle). The FWHM of the ^{32}S peak is 1.1 ns, which is approximately equal to the beam time resolution.

tion of the measured quantities for binary events. The resulting masses and velocity vectors are given by

$$m_1 = M_{\rm tot} \frac{\mathbf{v}_1^{\rm exp} \cdot (\mathbf{v}_2^{\rm exp} - \mathbf{v}_1^{\rm exp})}{|\mathbf{v}_2^{\rm exp} - \mathbf{v}_1^{\rm exp}|^2} , \quad (1)$$

$$\mathbf{v}_1 = \frac{\mathbf{v}_1^{\rm exp} - \mathbf{v}_2^{\rm exp}}{1 + m_1/m_2} , \quad (2)$$

where $\mathbf{v}_i^{\rm exp}$ $(i=1,2)$ corresponds to the experimentally measured center-of-mass velocity vectors for the two particles. Values of m_2 and $\mathbf{v}_2$ can be obtained by cyclic permutation of the indexes. In addition to the above calculations, an iterative event-by-event energy correction routine was utilized in order to compensate for target energy loss and angle straggling effects. Having determined the mass and velocity of the fission fragments, the total kinetic energy release (TKE) was calculated. Cuts in the resultant mass spectra were used to eliminate the chance coincidences between elastically scattered particles and γ rays from the γ-ray energy spectra.

The total γ-ray emission probability was approximated by the sums of coincidence spectra, measured by the top-bottom [$W(0°)$] and left-right [$W(90°)$] detector pairs, and were normalized to each other between 5 and 6 MeV. In heavy deformed nuclei the GDR γ-ray emission shows a strong angular correlation with respect to the spin axis of the CN [7] which is related to the shape parameter of the emitting system. Therefore, the γ-ray energy dependent angular anisotropies, $W(0°,E_\gamma)/W(90°,E_\gamma)$ were created from the γ-ray energy spectra at each bombarding energy.

Since the probability of detecting coincident fragments from a fission event depends on their mass and kinetic energy, it was necessary to determine the geometrical efficiency for each pair of PPAC's. This was accomplished by a Monte Carlo simulation of the fission process with the known detector geometry. The simulation generates a flat fragment mass distribution, isotropic emission of the fragments in the center-of-mass system and a Gaussian fragment total kinetic energy (TKE) distribution. The mean values for the fragment TKE distributions were taken from Viola systematics [9] and modified to allow for nonsymmetric fission events [10]. A resulting relative geometrical efficiency for the 185 MeV ^{32}S+$^{\rm nat}$W reaction is shown in Fig. 3. The calculations show somewhat higher probability of detecting asymmetric fission coincidence events at all beam energies. All γ-fission-fission coincidence data were corrected with the corresponding efficiency function. This reduces the measured width of the mass distribution by about 10%, but has no significant influence on the shape of the γ spectrum.

III. EXPERIMENTAL RESULTS

Figure 4 compares the present 140 MeV ^{16}O+^{208}Pb γ-ray energy spectra and angular correlations with that obtained in a prior measurement [1,2]. The reduced γ ray yield in the low-energy region (6–9 MeV) is the result of

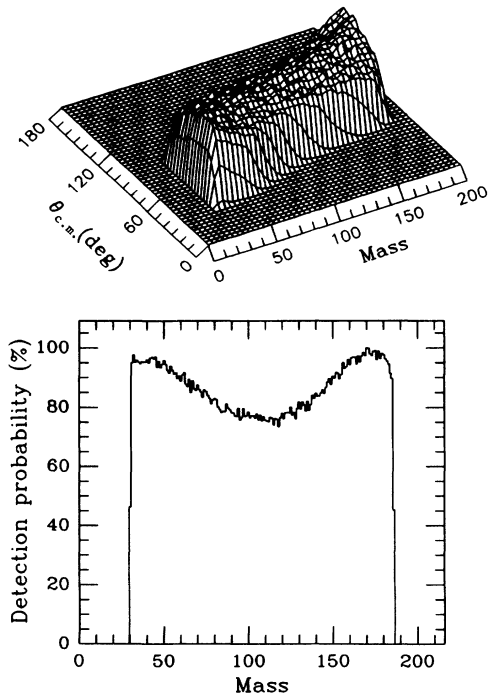

FIG. 3. The geometrical efficiency of the PPAC coincidence system as a function of $\theta_{\rm c.m.}$ scattering angle in the center-of-mass system and fission fragment mass for the ^{32}S+$^{\rm nat}$W reaction at 185 MeV.

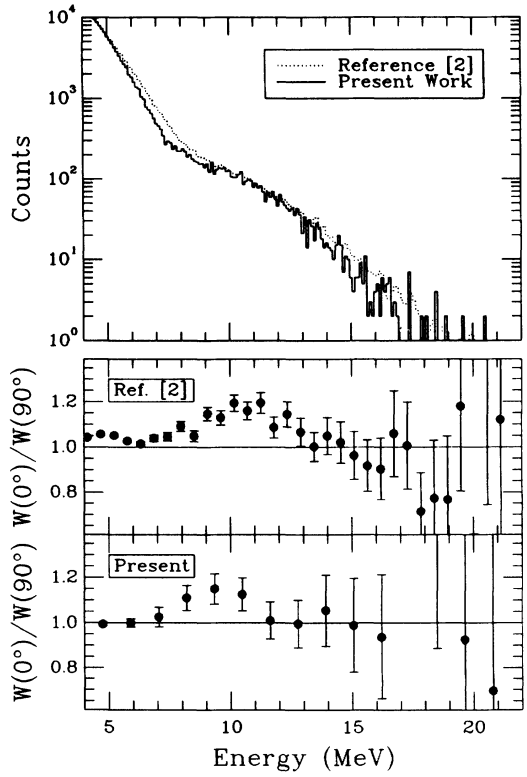

FIG. 4. Comparison of the γ-ray energy spectra and angular correlations from the present 140 MeV ^{16}O+^{208}Pb experiment with a prior measurement [2].

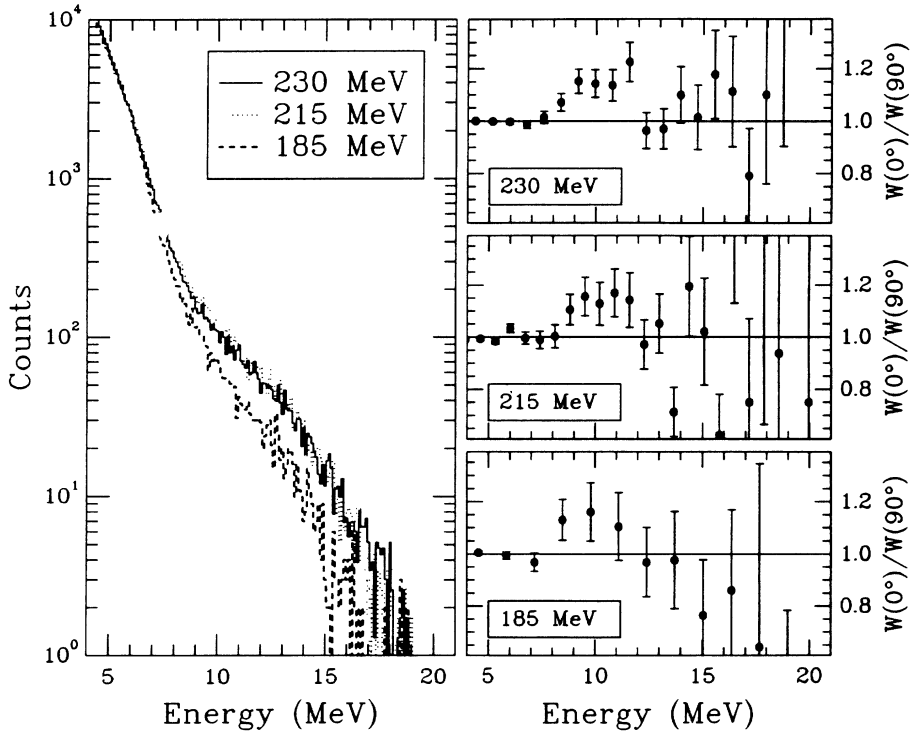

FIG. 5. Total γ-yield and γ-ray angular correlations with respect to the CN spin axis in the $^{32}S+^{nat}W$ reaction at 185, 215, and 230 MeV bombarding energy. The curves are normalized between $E_\gamma = 5$ and 6 MeV.

the improved neutron discrimination of the present setup. The two spectra are similar in the compound nucleus GDR energy region (9–14 MeV) and there is a small reduction in yield at higher energies ($E_\gamma > 14$ MeV). The latter may be due to the more restrictive γ-fission-fission triple coincidence requirement of the present experiment. The bottom part of Fig. 4 compares the angular correlation data from the two experiments. We note the shift of the correlation peak to somewhat lower energy, which is a consequence of the new spectrum shape.

Figure 5 shows the γ-ray energy spectra obtained from the $^{32}S+^{nat}W$ reaction in coincidence with the fission fragments at 185, 215, and 230 MeV bombarding energies. One observes a strong increase in the high-energy γ

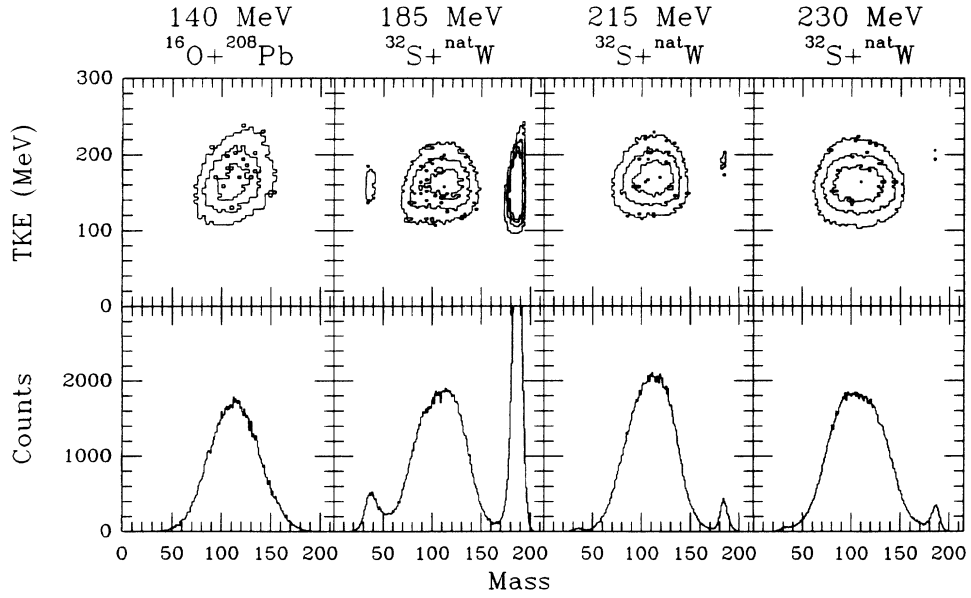

FIG. 6. Fission fragment mass and TKE distributions in the $^{16}O+^{208}Pb$ and $^{32}S+^{nat}W$ reaction at different bombarding energies.

yield when going from 185 to 215 MeV, but little additional change in the γ-ray energy spectrum shape from 215 to 230 MeV. The high-energy yield in the 185-MeV spectrum is somewhat higher, relative to the low-energy (5 to 6 MeV) region, than in the earlier measurement [2], due to the improved background discrimination. The right-side section of Fig. 5 displays the $^{32}S+^{nat}W$ angular correlations as a function of γ-ray energy. The anisotropy observed at all beam energies indicates the continued presence of the GDR γ rays from a long-lived deformed system.

Figure 6 presents the measured fission yields (in coincidence with γ rays) in contour plots of fragment mass vs total kinetic energy of both fission fragments (TKE) and the corresponding projections onto the mass axis. The data are integrated over the entire detector surface. The σ_A standard deviations of the mass distributions can be theoretically approximated [11] as $\sigma_A^2=(E^+/ak^2)^{1/2}$, where E^+ is the excitation energy of the system at the scission point, $a=A/8.8$ is the level density parameter, and k is the restoring force constant in the parabolic approximation of the mass asymmetry dependent potential energy surface at the scission point [11]. E^+ can be approximated as $E^+=E^*_{CN}+Q_f-TKE-E_{def}$, where E^*_{CN} is the excitation energy of the CN, Q_f is the Q value for the fission, TKE is the total kinetic energy release (approximated by the Kwiatkowski systematics [9]), and E_{def} is the deformation energy stored in the fission fragments (as an approximation $E_{def}=12$ MeV was taken). Figure 7 compares the measured σ_A standard deviations to the calculated values with $k=0.0035$ MeV/u^2 [11] (solid line) and $k=0.0061$ MeV/u^2 [3] (dashed line). The measured widths are somewhat larger than those of Ref. [3], but are in good agreement with the calculated values with $k=0.0035$ MeV/u^2.

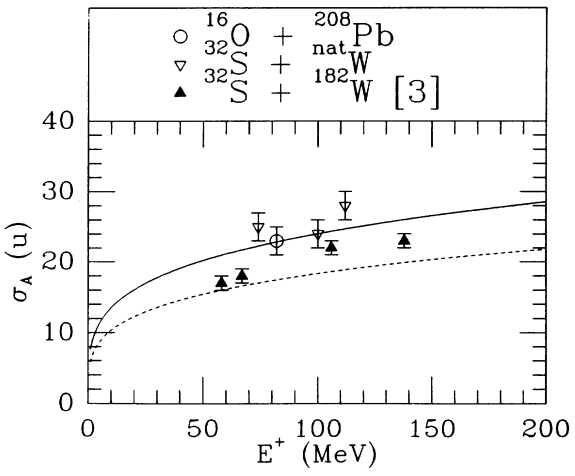

FIG. 7. The standard deviation of the fission fragment mass distribution as a function of the E^+ excitation energy at the scission point. The solid and dashed curves are calculated as given in the text.

IV. ANALYSIS AND DISCUSSION

A. $^{16}O+^{208}Pb$ reaction

At a bombarding energy of 140 MeV this reaction produces ^{224}Th at an initial nuclear temperature $T=1.8$ MeV. The statistical model code CASCADE [12], which was used in the present analysis of the CN decay had been extensively modified [2] to include the decay of excited fission fragments and the effects of nuclear dissipation in the fission degree of freedom. The dissipation mechanism is described by a time dependent fission decay width of

$$\Gamma_f(t)=\Gamma_f^{Kramers}\left[1-\exp\left[-\frac{t}{\tau_f}\right]\right], \quad (3)$$

where

$$\Gamma_f^{Kramers}=\Gamma_f^{BW}[(1+\gamma^2)^{1/2}-\gamma], \quad (4)$$

is the Kramers' solution [13] for the dissipative fission width. Γ_f^{BW} is the Bohr-Wheeler expression for the normal, nondissipative fission width, γ is the (normalized) nuclear friction coefficient, and τ_f is the fission delay time. The time of the saddle-to-scission motion is approximated by

$$\tau_{ssc}=\tau_{ssc}^0[(1+\gamma^2)^{1/2}+\gamma], \quad (5)$$

where τ_{ssc}^0 is the saddle-to-scission time without dissipation. This was calculated to be $\tau_{ssc}^0=3.0\times10^{-21}$ s [14]. It was shown that the parameter set $(\gamma,\tau_f,\tau_{ssc})$ contains only one independent parameter, the nuclear friction coefficient γ.

The GDR γ spectrum of the previous experiment was fitted well supposing a collective prolate shape of the system with $\beta=0.3$. A collective oblate shape is unambiguously excluded by the measured γ-ray angular correlation. At the temperature $T=1.8$ MeV, the CN may have changed its shape to a noncollective oblate shape. Such a transition has been recently observed in the $A=90$ mass region [15]. The liquid drop model (LDM) [16] predicts a noncollective oblate shape with average deformation of $\beta=-0.1$ for the Thorium CN at the present excitation energy. Therefore, an attempt was made to fit the data using the new CASCADE code (including the time dependent description of the fission hindrance effect) with a LDM noncollective oblate shape. Level densities ($a=A/8.8$ for the CN and $a=A/9.0$ for the fission fragment) were similar to earlier work [1]. The residue cross sections measured by Vulgaris *et al.* [17] at lower beam energy can be well reproduced without fission hindrance if one applies a multiplicative factor of 0.7 to the fission barriers of Sierk [18]; therefore, this factor was used in the present calculations. The width of the GDR was parametrized as $\Gamma_1/\Gamma_2=(E_1/E_2)^\delta$, with $\delta=1.9$ [19]. The top part of Fig. 8 shows the fit of the present data with GDR energies and widths listed in Table II, corresponding to noncollective oblate shape with the LDM deformation $\beta=-0.1$. We find that the calculation with nuclear friction coefficient $\gamma=10$ produces an excellent fit to the energy spectrum. The middle part displays the

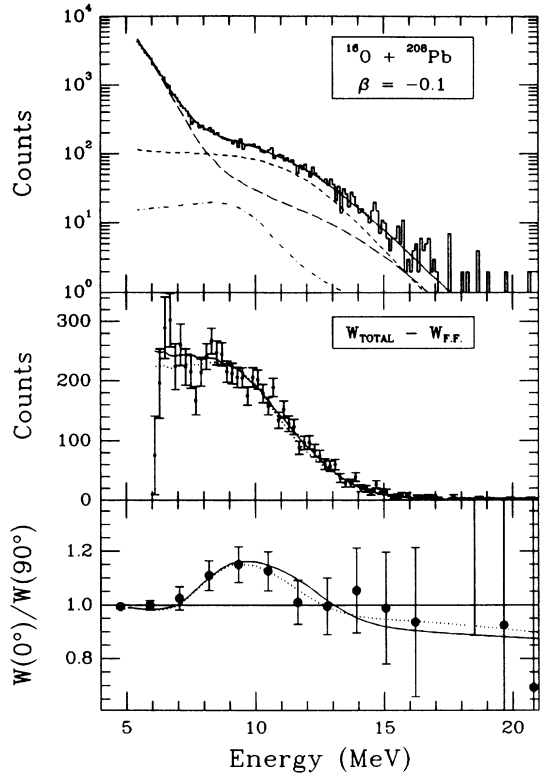

FIG. 8. Comparison of the 140 MeV $^{16}O+^{208}Pb$ data to CASCADE calculation. The input parameters are listed in Table II. Top part: The histogram represents the data; the solid line is the fit using a noncollective oblate shape (sum of the pre-saddle, saddle-to-scission, and post-scission γ-yields, shown as dashed, dash-dotted, and long-dashed lines, respectively). Middle part: Fit and data where the calculated fission yield has been subtracted. Bottom part: Angular correlation calculation and data. In the middle and bottom parts of the figure the solid and dotted lines correspond to prolate and noncollective oblate deformations, respectively.

data and the fit for the total γ yield, where the calculated fission fragment yield has been subtracted. The dotted line corresponds to a calculation with collective prolate deformation ($\beta=0.3$). One can observe that the shape of the γ-ray energy spectrum is practically the same with the two deformation parameters. The bottom part of Fig. 8 displays the measured anisotropy and the calculations corresponding to the two shapes. The calculations were performed using the formulas described in detail in Ref. [7]. We conclude on the basis of the present measurement that neither the prolate nor the noncollective oblate shape can be excluded, especially since the effect of shape fluctuations has not been included in the correlation calculations.

B. $^{32}S+^{nat}W$ reactions

The $^{32}S+^{nat}W$ reaction at bombarding energies of 185, 215, and 230 MeV forms the compound systems $^{214,216,218}Th$ at initial nuclear temperatures of 1.7, 2.0, and 2.1 MeV, respectively. This reaction has been shown to have a considerable amount of quasifission contribution to the total fission cross section [3]. In the quasifission process, the intermediate system is not completely equilibrated: the projectile is trapped behind a conditional saddle. The time scale of the process ($>10^{-20}$ s) can be long enough to emit neutrons, protons, even GDR γ rays.

In order to include the γ emission of the quasifission process, one can calculate [11,20] the extra-push energy E_x (additional projectile energy needed to create the relatively long-lived system called the mononucleus), and the extra-extra-push energy E_{xx} (still higher projectile energy needed to create the equilibrated CN) from

$$E_x = E_{ch} a^2 [(x'_{Bass})_{eq} - x_{th}]^2 , \quad (6)$$

$$E_{xx} = E_{ch} a^2 (x_m - x_{th})^2 , \quad (7)$$

where E_{ch} is a characteristic energy, $(x'_{Bass})_{eq}$ is an effective fissility, and x_m is a scaling parameter. The value of the slope parameter a and the threshold parameter x_{th} were taken as $a=7.3$ and $x_{th}=0.62$ from Ref. [11].

Figure 9 shows the calculated extra-push and extra-extra-push energies as a function of the compound system angular momentum (l). Also displayed are the projectile energies above the (l dependent) interaction barrier [21]. In the $^{32}S+^{nat}W$ reaction, depending on the l value, the CN is formed for more central collisions, and the mononucleus for higher partial waves. For very high l values there is not enough energy to make any long-lived

TABLE II. Compound nucleus GDR parameters used in the CASCADE calculations for prolate and noncollective oblate shapes. The noncollective oblate deformations correspond to the LDM predictions for the average angular momentum of the CN.

			CN GDR Parameters					
Reaction	E_{lab}	β	E_1	Γ_1	S_1	E_2	Γ_2	S_2
$^{16}O+^{208}Pb$	140	0.3	11.0	4.2	1/3	14.0	5.8	2/3
		−0.1	12.1	5.5	2/3	13.3	6.5	1/3
$^{32}S+^{nat}W$	185	0.3	11.0	4.2	1/3	14.0	5.8	2/3
		−0.2	12.6	5.5	2/3	12.8	5.7	1/3
	215	0.3	11.0	5.7	1/3	14.0	7.3	2/3
		−0.07	12.4	6.0	2/3	13.3	6.9	1/3
	230	0.3	11.0	6.6	1/3	14.0	8.2	2/3
		−0.08	12.3	6.5	2/3	13.3	7.5	1/3

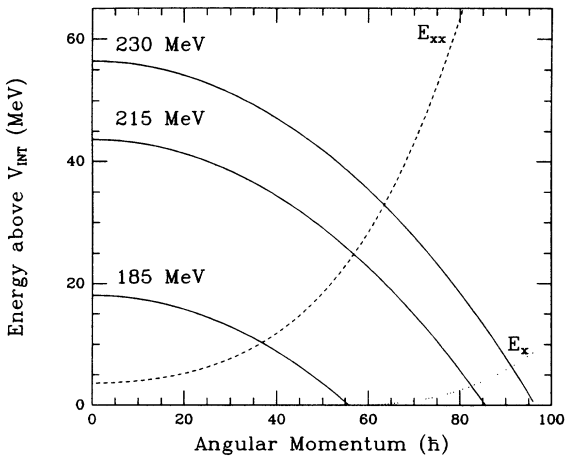

FIG. 9. Results of an extra-push model calculation. E_x and E_{xx} are the extra-push and extra-extra-push energies, and the solid lines correspond to the energy above the interaction barrier for 185, 215, and 230 MeV.

system. The crossing points of the E_{xx} curve with the curves representing the projectile energies above the interaction barrier determine the limiting l_{QF} values. If $l < l_{QF}$, the CN, if $l > l_{QF}$, the mononucleus is formed. If one assumes the standard spin population for heavy-ion reactions, the l_{QF} value obtained from the extra-push model directly gives the cross sections of the CN and mononucleus formation, respectively. Table III shows the corresponding cross sections extracted from Fig. 9 along with the values interpolated from the experimental results of Ref. [3].

Using the extra-push model as a picture for the quasifission process, the statistical model calculations were done as follows. For $l < l_{QF}$, where the energy is high enough to create the compound nucleus, a normal statistical calculation is done including the effects of fission hindrance, saddle-to-scission decay and subsequent fragment γ decay. Level density parameters and the fission barrier multiplicative factor for this part of the $^{32}S+^{nat}W$ calculations were taken to be the same as in $^{16}O+^{208}Pb$ reaction, since approximately the same compound system is created. Since one can suppose either prolate deformation or noncollective oblate deformation, two sets of calculations were performed. Table II summarizes the CN GDR energy parameters used for prolate ($\beta=0.3$) and noncollective oblate shapes from the liquid drop model predictions [16]. The width of the GDR for calculations with prolate shape was obtained from [4] $\Gamma = A + BE^{\delta}$ relation, where $B=0.0026$, $\delta=1.6$, and A is determined from the measurement [2]. For values of $l > l_{QF}$ the mononucleus is formed. Its decay is treated as consisting only of a saddle-to-scission decay with a quasifission lifetime τ_{QF} (which is different from the τ_{ssc} saddle-scission decay time) and the subsequent fragment decay. The mononucleus has an elongated prolate shape; therefore the GDR energy splitting should be larger than that of the CN. For the 185 MeV $^{32}S+^{nat}W$ reaction, the mononucleus GDR energy and strengths parameters were taken to be $E_1=9.8$ MeV, $\Gamma_1=2.5$ MeV, and $E_2=15.5$ MeV, $\Gamma_2=5.0$, $S_1=1/3$, $S_2=2/3$, corresponding to a prolate deformation value of $\beta=0.56$ [2]. for a starting value of the mononucleus excitation energy an average of the thermal excitation energies at the saddle and scission point $E^*_{mon}=0.5(U_{saddle}+U_{scission})$ was taken [22]. For the three ^{32}S beam energies of 185, 215, and 230 MeV this value corresponds to $E^*_{mon}=67$, 87, and 98 MeV, respectively. The quasifission lifetime was initially estimated to be $\tau_{QF}=2\times10^{-20}$ [11].

Figure 10 shows CASCADE γ-spectra predictions supposing a prolate shape for all three energies calculated with three different assumptions: (1) a quasifission calculation as outlined above; (2) a CN calculation including fission hindrance; and (3) a CN calculation without fission hindrance. The calculations are folded with the NaI detector response function [4]. The difference between the calculations without hindrance (3) and with hindrance (2) is clearly large enough to be experimentally observable. The difference in the γ yield between the CN hindrance (2) and the quasifission (1) calculation (displayed in the bottom part of Fig. 10) is about 20% in the GDR energy region (at about 12 MeV) for the 185 MeV bombarding energy. This difference is reduced at higher energies because a larger portion of the fusion cross section corresponds to partial waves l for which the fission barrier vanishes. Therefore the 185 MeV data was chosen for a more detailed analysis of the influence of quasifission effects on the γ spectra and used to determine the most probable parameter values.

TABLE III. Published results for quasifission strength in the reaction $^{32}S+^{nat}W\rightarrow{}^{\sim216}Th$. The columns list the beam energy, the effective beam energy at the center of the target, and three sets of cross sections for complete fusion (σ_{CN}), quasifission (σ_{QF}), and the corresponding quasifission spin cut (l_{QF}).

		Keller[a]			Glagola[b]			Extra push[c]		
E_{beam} (MeV)	E^{eff}_{beam} (MeV)	σ_{CN} (mb)	σ_{QF} (mb)	l_{QF} ($\hbar$)	σ_{CN} (mb)	σ_{QF} (mb)	l_{QF} ($\hbar$)	σ_{CN} (mb)	σ_{QF} (mb)	l_{QF} ($\hbar$)
185	181	342	125	47	202	247	36	220	280	38
215	211	505	312	61	421	304	56	443	491	57
230	226	572	402	68	579	425	68	520	550	64

[a]Keller *et al.* [3].
[b]Data taken by Glagola *et al.* [24] and reanalyzed by Keller *et al.* [3].
[c]Predictions from the extra-push model [20] using the formalism and parameters from Shen *et al.* [11].

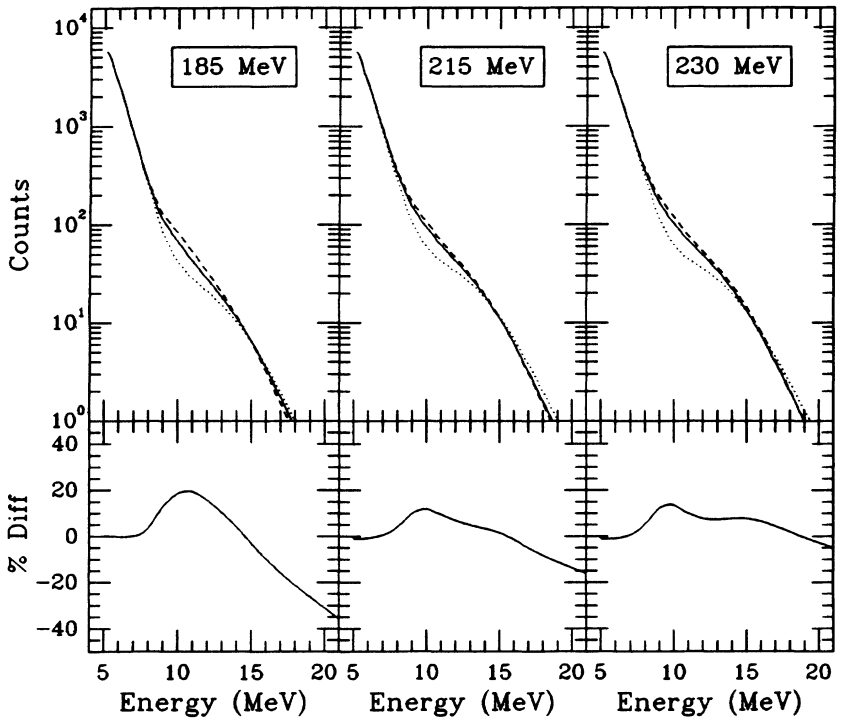

FIG. 10. CASCADE calculations for the 185, 215, and 230 MeV $^{32}S+^{nat}W$ reaction with different assumptions. (1) Solid line: quasifission calculation, including the effect of fission hindrance. (2) Dashed line: calculation with fission hindrance, but without quasifission. (3) Dotted line: calculation without fission hindrance and quasifission effects. Bottom part: relative difference of the spectra (1−2)/1.

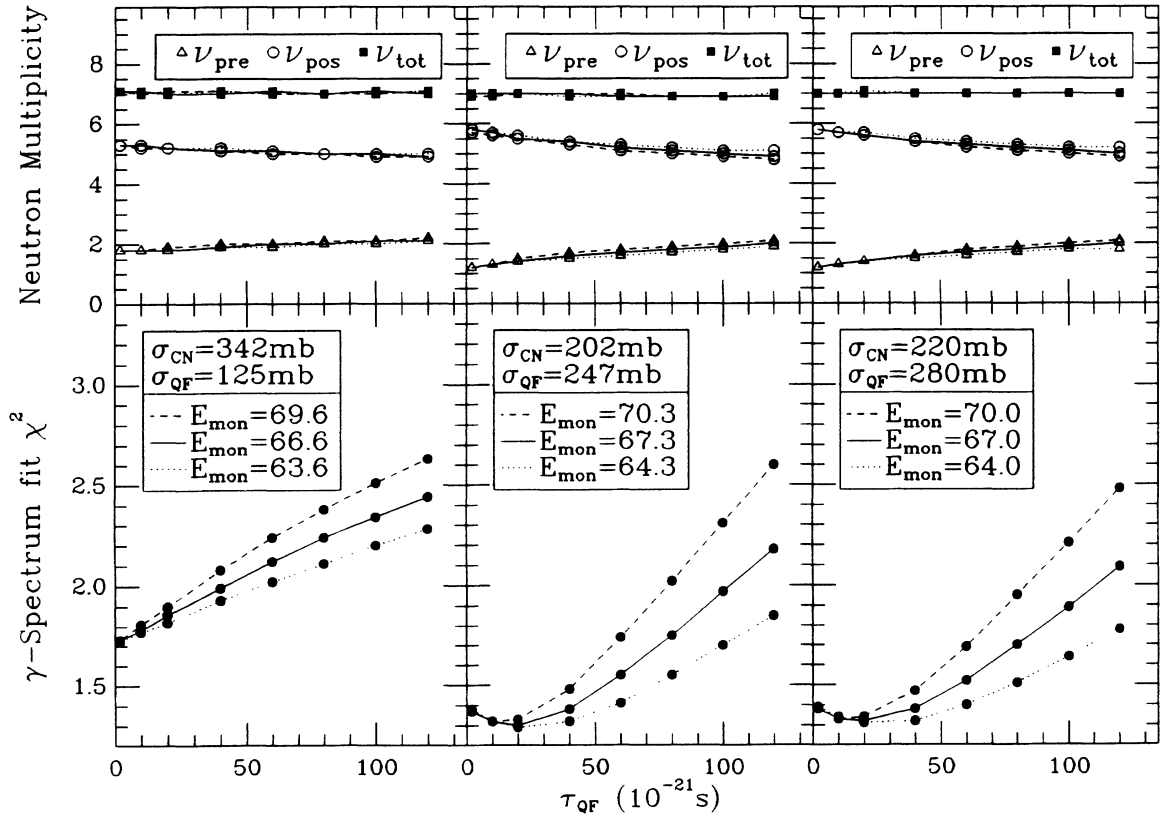

FIG. 11. χ^2 analysis for the quasifission lifetime and calculated pre-saddle (ν_{pre}), post-saddle (ν_{pos}) and total (ν_{tot}) neutron multiplicities for three sets of σ_{CN} and σ_{QF} values ($\sigma_{fiss}=\sigma_{CN}+\sigma_{QF}$). The first two sets are from [3], the third (rightmost) was calculated from the extra-push model using the parameters of [11]. The calculations were performed for three different average mononucleus excitation energies E_{mon}.

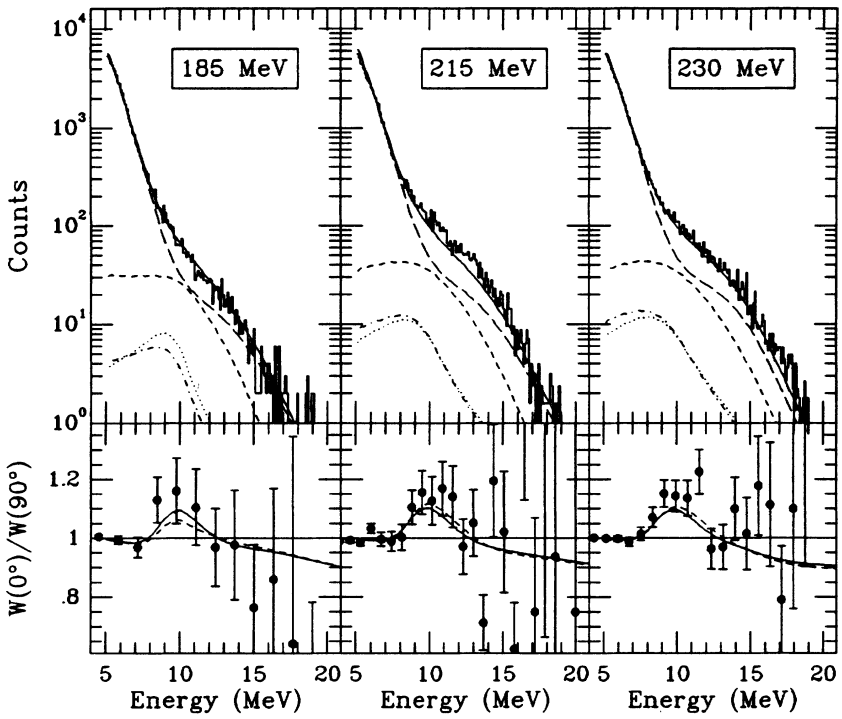

FIG. 12. Comparison of the $^{32}S+^{nat}W$ data to CASCADE calculations. Upper part: Fit of the γ spectra, using the quasifission calculation with prolate deformation of the CN. The histogram represents the data; the solid line is the sum of the calculated pre-saddle, saddle to scission, quasifission, and post-scission γ yields, shown as dashed, dash-dotted, dotted, and long-dashed lines, respectively. Lower part: angular correlation calculation and data. The solid and dashed lines correspond to prolate and noncollective oblate deformations of the CN, respectively.

A χ^2 analysis was performed in order to extract the most probable value of the quasifission lifetime, τ_{QF}. The fits were done using the three available cross section data sets shown in Table III and for three different average excitation energies of the mononucleus (E^*_{mon}). These energies in fact cover the whole region of the allowed E^*_{mon} values for the average spin value of the mononucleus. Reduced χ^2 values were obtained from comparison of the fits to the data in the GDR γ-ray energy region of 8–25 MeV and are plotted in Fig. 11. Also shown are the corresponding precision (ν_{pre}), post-scission (ν_{pos}) and total (ν_{tot}) neutron multiplicities as given by CASCADE. An absolute minimum in the χ^2 could be obtained when at least 55% of the fission cross section was due to quasifission. In this case the most probable quasifission lifetime value is $\tau_{QF}=(20-40)\times10^{-21}$ s. Varying the mononucleus excitation energy, E^*_{mon}, does not change the most probable value of τ_{QF} considerably. The ν_{pre} and ν_{pos} pre-saddle and post-saddle neutron multiplicities show a slight change with τ_{QF}, whereas the total neutron multiplicity ν_{tot} remains constant.

The quasifission fits for 215 and 230 MeV bombarding energies were done using cross-section values from the extra-push model. Since the calculated $\sigma_{QF}/\sigma_{fiss}$ ratio is $\sim$50% for all three bombarding energies, the quasifission lifetime was kept as $\tau_{QF}=20\times10^{-21}$ s.

The upper part of Fig. 12 compares the calculated and measured γ spectra supposing the prolate deformation of the CN. All the calculations were done using $\gamma=10$ nuclear friction coefficient and resulted in good fits of the 185 and 230 MeV data. For 215 MeV the fit is less accurate. In order to improve the fit one would have to increase the nuclear friction parameter even more, or alternatively use narrower widths for the GDR. Comparing the different γ sources one can observe a relatively large increase in the saddle to scission and mononucleus γ yield (dash-dotted and dotted lines) as the beam energy increases. Calculations with GDR parameters corresponding to LDM predictions for noncollective oblate deformations of the CN resulted in practically identical shapes of the total γ spectra and therefore are not shown in the figure. The bottom part of Fig. 12 compares the $W(0°,E_\gamma)/W(90°,E_\gamma)$ angular correlation data to the calculations. Within the large error bars the data and the calculations are in agreement. The difference in the magnitude of the correlations corresponding to prolate or noncollective oblate shapes of the CN is small, therefore the shape cannot be unambiguously determined from the present experiment.

V. SUMMARY AND CONCLUSIONS

This experiment is the first in which GDR γ rays in a hot nucleus are measured in kinematic coincidence with both fission fragments. The widths of the observed mass distribution of the fission fragments in coincidence with GDR γ rays show the same width as that without coincidence. The GDR spectra measured in the $^{16}O+^{208}Pb$ reaction reconfirm the earlier result of a surprisingly large nuclear viscosity ($\gamma=10$) for the large-scale nuclear mass flow involved in fission of ^{224}Th at temperatures $T\approx1.8$ MeV.

As in the earlier work, the GDR γ-ray angular correlation relative to the nuclear spin axis shows the presence of a strongly deformed nuclear system. The measured GDR γ-ray spectrum and correlation is well described assuming a large prolate deformation ($\beta=0.3$) similar to the ground state deformation of ^{232}Th. On the other

hand, it is also explained by a noncollective oblate shape ($\beta=-0.1$) which corresponds to the rotating liquid drop deformation. It is thus possible that the transition from the prolate deformation of the ground state to the noncollective oblate deformation, which is expected to occur somewhere at a temperature $T=1.7-2.1$ MeV, has in fact occurred. But to prove this conjecture requires much better statistics.

One of the main motivations of this experiment was a detailed investigation of the effect of the quasifission reaction mechanism on the GDR γ-ray spectrum in the $^{32}S+^{nat}W$ reaction. Model calculations show that the quasifission process, when present, leads to a reduction of high-energy GDR γ rays, relative to the low-energy part of the spectrum dominated by fission fragments, at 185 MeV bombarding energy. At the higher bombarding energies the GDR spectrum becomes relatively insensitive to the differences between CN fission and quasifission. It would require a selection by angular momentum to improve the situation. Including the GDR γ rays emitted from the intermediate system, the mononucleus, prior to quasifission in an approximate way results in a successful fit of the data at 185 and 230 MeV bombarding energies, whereas at 215 MeV the fit slightly underpredicts the data. In all cases in the $^{32}S+^{nat}W$ reaction we again observe a large viscosity ($\gamma=10$) of the nuclear material. A χ^2 analysis of the data determines the most probable value of the quasifission lifetime as $\tau_{QF}=(20-40)\times10^{-21}$ s, about ten times shorter than the hindered CN fission of the hot ^{224}Th nucleus.

ACKNOWLEDGMENTS

The authors are indebted to M. Thoennessen for the valuable discussions on the use of the modified CASCADE codes. This work was supported in part by the National Science Foundation.

[1] M. Thoennessen, D. R. Chakrabarty, M. G. Herman, R. Butsch, and P. Paul, Phys. Rev. Lett. **59**, 2860 (1987).
[2] R. Butsch, D. J. Hofman, C. P. Montoya, P. Paul, and M. Thoennessen, Phys. Rev. C **44**, 1515 (1991).
[3] J. G. Keller, B. B. Back, B. G. Glagola, D. Henderson, S. B. Kaufman, S. J. Sanders, R. H. Siemssen, F. Videbaek, B. D. Wilkins, and A. Worsham, Phys. Rev. C **36**, 1364 (1987).
[4] D. R. Chakrabarty, S. Sen, M. Thoennessen, N. Alamanos, P. Paul, R. Schicker, J. Stachel, and J. J. Gaardhøje, Phys. Rev. C **36**, 1886 (1987).
[5] I. Diószegi, D. J. Hofman, and P. Paul, Nucl. Instrum. Methods (to be submitted).
[6] S. Sen, D. R. Chakrabarty, P. Paul, J. Stachel, and M. Thoennessen, Nucl. Instrum. Methods **A264**, 407 (1988).
[7] R. Butsch, M. Thoennessen, D. R. Chakrabarty, M. G. Herman, and P. Paul, Phys. Rev. C **41**, 1530 (1990).
[8] G. Casini, P. R. Maurenzig, A. Olmi, and A. A. Stefanini, Nucl. Instrum. Methods **A277**, 445 (1989).
[9] V. E. Viola, K. Kwiatkowski, and M. Walker, Phys. Rev. C **31**, 1550 (1985).
[10] R. Bock, Y. T. Chu, M. Dakowski, A. Gobbi, E. Grosse, A. Olmi, H. Sann, D. Schwalm, U. Lynen, W. Müller, S. Bjørnholm, H. Esbensen, W. Wölfli, and E. Morenzoni, Nucl. Phys. **A388**, 334 (1982).
[11] W. Q. Shen, J. Albinski, A. Gobbi, S. Gralla, K. D. Hildenbrand, N. Herrmann, J. Kuzminski, W. F. J. Müller, H. Stelzer, J. Toke, B. B. Back, S. Bjørnholm, and S. P. Sørensen, Phys. Rev. C **36**, 115 (1987).
[12] F. Pühlhofer, Nucl. Phys. **A260**, 276 (1977).
[13] H. A. Kramers, Physica **7**, 284 (1940).
[14] J. R. Nix, Nucl. Phys. **A130**, 241 (1969).
[15] J. H. Gundlach, K. A. Snover, J. A. Behr, C. A. Gossett, and M. Kicinska-Habior, Phys. Rev. Lett. **20**, 2523 (1990).
[16] S. Cohen, F. Plasil, and W. J. Swiatecki, Ann. Phys. (N.Y.) **82**, 557 (1974).
[17] E. Vulgaris, L. Grodzins, S. G. Steadman, and R. Ledoux, Phys. Rev. C **33**, 2017 (1986).
[18] A. J. Sierk, Phys. Rev. C **33**, 2039 (1986).
[19] N. Gallardo, F. J. Luis, and R. A. Broglia, Phys. Lett. B **191**, 222 (1987).
[20] S. Bjørnholm and W. J. Swiatecki, Nucl. Phys. **A391**, 471 (1982).
[21] B. B. Back, R. R. Betts, J. E. Gindler, B. D. Wilkins, S. Saini, M. B. Tsang, C. K. Gelbke, W. G. Lynch, M. A. McMahan, and P. A. Baisden, Phys. Rev. C **32**, 195 (1985); **33**, 385 (1986).
[22] D. J. Hinde, H. Ogata, M. Tanaka, T. Shimoda, N. Takahashi, A. Shinohara, S. Wakamatsu, K. Katori, and H. Okamura, Phys. Rev. C **39**, 2268 (1989).
[23] F. Videbaek, R. B. Goldstein, L. Grodzins, S. G. Steadman, T. A. Belote, and J. D. Garrett, Phys. Rev. C **15**, 954 (1977).
[24] B. G. Glagola, B. B. Back, R. R. Betts, and B. D. Wilkins, Bull. Am. Phys. Soc. **26**, 550 (1981).